

An alternative GPU acceleration for a pseudopotential plane-waves density functional theory code with applications to metallic systems

Xuejun Gong^{a,b,*}, Andrea Dal Corso^{a,b}

^a*International School for Advanced Studies(SISSA), Via Bonomea 265, Trieste, Italy, 34136*

^b*CNR-IOM, Via Bonomea 265, Trieste, Italy, 34136*

Abstract

We present an alternative GPU acceleration for plane waves pseudopotentials electronic structure codes designed for systems that have small unit cells but require a large number of \mathbf{k} points to sample the Brillouin zone as happens, for instance, in metals. We discuss the diagonalization of the Kohn and Sham equations and the solution of the linear system derived in density functional perturbation theory. Both problems take advantage from a rewriting of the routine that applies the Hamiltonian to the Bloch wave-functions to work simultaneously (in parallel on the GPU threads) on the wave-functions with different wave-vectors \mathbf{k} , as many as allowed by the GPU memory. Our implementation is written in CUDA Fortran and makes extensive use of kernel routines that run on the GPU (GLOBAL routines) or can be called from inside the GPU threads (DEVICE routines). We compare our method with the CPUs only calculation and with the approach currently implemented in Quantum ESPRESSO that uses GPU accelerated libraries for the FFT and for the linear algebra tasks such as the matrix-matrix multiplications as well as OpenACC directives for loop parallelization. We show in a realistic example that our method can give a significant improvement in the cases for which it has been designed.

Keywords: Electronic structure; Lattice dynamics; Metals; GPU; Density functional perturbation theory.

*Corresponding author.
E-mail address: xgong@sissa.it

Contents

| | | |
|----------|--|-----------|
| 1 | Introduction | 2 |
| 2 | Theory | 5 |
| 2.1 | Davidson algorithm | 5 |
| 2.2 | Application of Hamiltonian | 7 |
| 2.2.1 | Kinetic energy | 7 |
| 2.2.2 | Local potential | 8 |
| 2.2.3 | Non local pseudopotential and overlap matrix | 8 |
| 2.3 | Density functional perturbation theory | 9 |
| 2.4 | Preconditioned conjugate gradient | 11 |
| 3 | GPU optimization | 12 |
| 4 | Fast Fourier transform | 17 |
| 4.1 | FFT on the device | 19 |
| 5 | Matrix Diagonalization | 20 |
| 6 | Results | 21 |
| 6.1 | Benchmark Example | 21 |
| 6.2 | FFT | 22 |
| 6.3 | Diagonalization | 23 |
| 6.4 | Application of the Hamiltonian and of S | 24 |
| 6.5 | Total time | 25 |
| 7 | Conclusions and perspectives | 26 |
| 8 | Appendix: GPU and CUDA Fortran | 28 |
| 9 | Acknowledgments | 29 |

1. Introduction

Density functional theory [1] (DFT) and the availability of more and more powerful computers has made the study of material properties from first-principles a well established reality. Several tools have been refined over

the years to solve the one electron Kohn and Sham equations that derive from DFT, [2] the most widespread being based on a plane waves basis and pseudopotentials. Well tested, freely available [3, 4, 5] or commercial [6, 7] packages implement the theory and allow the calculation of material properties.

In the last ten years, high performance computers aiming to reach the exaflops (10^{18} floating point operations per second) switched to a hybrid technology in which the graphic processing units (GPUs) support the central processing units (CPUs) in the floating point operations. In theory, the GPUs can deliver one or two orders of magnitude more flops than the CPUs themselves, and to harness this power many electronic structure groups are modifying their codes to run on the GPUs. [8, 9, 10, 11, 12, 13]

Extensions of common programming languages such as C/C++ or Fortran have provided commands to allocate data on the GPU, to move data from the CPU to the GPU and vice versa, and to perform calculations on these data with the GPU. CUDA Fortran commands, [14] declarations, and compiler directives and OpenACC compiler directives [15] are two of the most commonly used Fortran extensions. Recently also applications based on openMP started to appear in the literature. [16, 17] Actually OpenACC and OpenMP have the additional benefit of being transferable to GPUs architectures of different vendors such as NVIDIA, AMD, or Intel and sometimes are preferred to CUDA Fortran that is limited to NVIDIA GPUs.

So far, in several plane-waves pseudopotentials and quantum chemistry codes, the GPUs have been exploited by allocating the variables on the GPU and by substituting the calls to linear algebra and fast Fourier transform (FFTs) routines with calls to optimized library routines (such as cuBlas, [18] cuSolver, [19] cuFFT, [20] and MAGMA [21]) developed by the GPUs vendors and capable to run on the GPU. [22, 9, 16, 23, 24, 25] Sometimes the routines of these libraries have the same names and arguments of the corresponding CPU libraries and it suffices to allocate the variables on the GPU to call the GPU routines with minimal changes to the underlying codes and algorithms. Single loops using variables allocated on the GPUs can also be accelerated by compiler directives.

In Quantum ESPRESSO [3, 4] work on this kind of acceleration started more than ten years ago [26] and has been improved over the years [27] leading to a well tested package. [9] Accelerations of 2X or higher with respect to the CPU are often found in pseudopotential plane waves codes that adopt this approach. However, test systems are usually big supercells with many

atoms for which the time spent to make calculations on the GPU is larger than the time needed to transfer data from the CPU to the GPU, while small size systems are left out from these tests. For some applications, metallic systems with small unit cells need tens or hundreds thousands \mathbf{k} points to sample the Fermi surface. [28, 29, 30, 31, 32, 33, 34, 35, 36] The calculation of the phonon dispersions of these systems for many geometries as required for thermodynamic calculations is a problem that could take advantage from the new supercomputers, but for small systems we found that the use of the GPUs with the present codes is not always convenient and sometimes it can also slow down the calculation with respect to the CPUs alone.

We have therefore tried to improve the situation and in this paper we present the solution that we have found: an alternative approach to the acceleration of the pseudopotentials plane waves codes that is useful to deal with metallic system when there are many \mathbf{k} points. We load on the GPU many wave-functions (i.e. \mathbf{k} points), all the available ones if the GPU memory is large enough or as many as possible until there is free GPU memory. Then we make the calculations simultaneously on all these data (application of the Hamiltonian to the wave-functions) with each GPU thread working on a single wave-function or on a part of it. To obtain the precise control of the GPU threads that is needed we wrote a set of kernel functions (called GLOBAL in the CUDA language) that implement the theory and run on the GPU. These kernel functions need to call linear algebra and FFT library functions from inside the GPU threads. Unfortunately, libraries such as cuFFT, cuSolver, or MAGMA, which are called from the CPU and automatically control the number of threads, are not suited for our algorithm. We need functions that can be called from inside the GPU threads (DEVICE functions in the CUDA language). We only find the C++ library cuFFTDx [37] that implements such functionalities, but it does not provide a FORTRAN interface so far. For the moment, we transformed to the DEVICE form the FORTRAN sources of fftpack5.1 and of selected LAPACK routines. Finally, we obtained a code significantly faster than the standard one for small systems with many \mathbf{k} points.

We start with a brief introduction of the main equations that are solved in a plane-waves pseudopotential code. We stress in particular the algorithms that are relevant for the following discussion, neglecting the parts that have not changed or that are still calculated on the CPU. We then discuss how, in our method, the different parts of the code have been accelerated on the GPU. Finally, we present a test of our implementation and compare the times required by our approach with those taken by the CPUs only calculations and

by the previously available GPU implementation.

2. Theory

The solutions of the Kohn and Sham (KS) equations minimize the DFT total energy. These equations are an eigenvalue problem for norm conserving pseudopotentials, [38] and a generalized eigenvalue problem for ultrasoft [39] or projector-augmented wave (PAW) pseudopotentials. [40, 41] For periodic solids they can be written as:

$$H_{KS}\psi_{\mathbf{k}\nu} = \varepsilon_{\mathbf{k}\nu}S\psi_{\mathbf{k}\nu}, \quad (1)$$

where \mathbf{k} is a wave vector and ν is a band index. H_{KS} is the Kohn and Sham Hamiltonian and S is the overlap matrix. We are interested in finding the lowest N_b (number of bands) eigenvalues and eigenvectors of these equations. The Kohn and Sham Hamiltonian depends itself from a potential that is calculated from the charge density (that also depends on the wavefunctions). It is possible to solve this problem by a self-consistent procedure in which the wavefunctions are first calculated with an approximate potential. Then these wavefunctions are used to recompute the charge density and a new potential. The latter is mixed with the potential of the previous iterations and the procedure is repeated until one reaches self-consistency. At each step of the procedure however one has to diagonalize a fixed Hamiltonian which is progressively improved.

In the standard algorithm the problem is solved sequentially for each \mathbf{k} vector and the charge density is computed at the end when all wave-functions are available.

2.1. Davidson algorithm

There are several algorithms currently implemented in electronic structure codes to find the eigenvalues and eigenfunctions in Eq. 1, but here we limit the discussion to the Davidson algorithm. [42] In this algorithm an initial set of N_b functions $|\phi_i^{(n)}\rangle$ are progressively improved by enlarging the set applying $H_{KS} - \varepsilon_i S$ and solving the generalized eigenvalue problem $\tilde{H}_{ij} - \varepsilon \tilde{S}_{ij}$ on the basis formed by the original and the newly calculated vectors. A standard software library for numerical linear algebra, such as LAPACK, [43] is employed for the diagonalization. The algorithm is the following and has to be repeated for each \mathbf{k} point:

- Given N_b trial eigenpairs: $\left\{ \left| \phi_i^{(n)} \right\rangle, \varepsilon_i^{(n)} \right\}$ of the reduced Hamiltonian calculate:

$$\tilde{H}_{ij} = \left\langle \phi_i^{(n)} \left| H_{KS} \right| \phi_j^{(n)} \right\rangle, \quad \tilde{S}_{ij} = \left\langle \phi_i^{(n)} \left| S \right| \phi_j^{(n)} \right\rangle. \quad (2)$$

- Build the correction vectors $\left| \tilde{\phi}_i^{(n)} \right\rangle$:

$$\left| \tilde{\phi}_i^{(n)} \right\rangle = \left(H_{diag} - \varepsilon_i^{(n)} S_{diag} \right)^{-1} \left(H_{KS} - \varepsilon_i^{(n)} S \right) \left| \phi_i^{(n)} \right\rangle, \quad (3)$$

where H_{diag} and S_{diag} are the diagonal elements of H_{KS} and S in the plane waves representation.

- Normalize the correction vectors:

$$\left| \tilde{\phi}_i^{(n)} \right\rangle = \frac{\left| \tilde{\phi}_i^{(n)} \right\rangle}{\sqrt{\left\langle \tilde{\phi}_i^{(n)} \left| \tilde{\phi}_i^{(n)} \right\rangle}}. \quad (4)$$

- Build an extended reduced Hamiltonian and overlap matrix:

$$\tilde{H}_{ij} = \left\langle \phi_i^{(n)} / \tilde{\phi}_i^{(n)} \left| H_{KS} \right| \phi_j^{(n)} / \tilde{\phi}_j^{(n)} \right\rangle, \quad \tilde{S}_{ij} = \left\langle \phi_i^{(n)} / \tilde{\phi}_i^{(n)} \left| S \right| \phi_j^{(n)} / \tilde{\phi}_j^{(n)} \right\rangle. \quad (5)$$

- Set N_{base} equal to the number of basis vector. Diagonalize the small $N_{base} \times N_{base}$ reduced Hamiltonian to get the new estimate for the lowest N_b eigenpairs:

$$\left(\tilde{H} - \varepsilon \tilde{S} \right) v = 0 \quad \longrightarrow \quad \left\{ \left| \phi_i^{(n+1)} \right\rangle, \varepsilon_i^{(n+1)} \right\}. \quad (6)$$

- Calculate $\left| \tilde{\phi}_i^{(n+1)} \right\rangle$ for all i for which $\left| \varepsilon_i^{(n+1)} - \varepsilon_i^{(n)} \right| > \varepsilon_{th}$ where ε_{th} is the accuracy required for the eigenvalues and call N_{nc} the number of new vectors.
- If $N_{nc} > 0$ repeat with the basis $\left| \phi_i^{(n)} / \tilde{\phi}_i^{(n)} / \tilde{\phi}_i^{(n+1)} \right\rangle$ of size $N_{base} + N_{nc}$ and continue with progressively larger basis. When the size of the basis becomes too large for the allocated memory instead of adding $\left\{ \left| \tilde{\phi}_i^{(n+1)} \right\rangle \right\}$ to the basis, restart with $\left\{ \left| \phi_i^{(n+1)} \right\rangle, \varepsilon_i^{(n+1)} \right\}$. If $N_{nc} = 0$ exit with eigenpairs $\left\{ \left| \phi_i^{(n+1)} \right\rangle, \varepsilon_i^{(n+1)} \right\}$

The most time consuming step of this algorithm is the application of the operators H_{KS} and S to the wave-functions as discussed in the next subsection.

2.2. Application of Hamiltonian

The KS Hamiltonian can be written as: [44]

$$H_{KS}\psi_{\mathbf{k}\nu} = \underbrace{-\frac{1}{2}\nabla^2\psi_{\mathbf{k}\nu}}_{\text{kinetic energy}} + \underbrace{V_{eff}\psi_{\mathbf{k}\nu}}_{\text{local energy}} + \underbrace{V_{NL}\psi_{\mathbf{k}\nu}}_{\text{non-local energy}}, \quad (7)$$

where the effective potentials is the sum of the local, Hartree, and exchange and correlation potentials:

$$V_{eff} = V_{loc} + V_H + V_{XC}, \quad (8)$$

while the nonlocal pseudopotential is defined in term of the projector functions $|\beta_m^I\rangle$ and pseudopotential coefficients D_{mn}^I : [38, 39]

$$V_{NL}|\psi_{\mathbf{k}\nu}\rangle = \sum_{Imn} D_{mn}^I |\beta_m^I\rangle \langle \beta_n^I | \psi_{\mathbf{k}\nu}\rangle. \quad (9)$$

Here I indicates the different atoms in the solid and m and n run on all the β_m^I functions of a given atom.

The overlap matrix can be calculated in a similar way: [39]

$$S|\psi_{\mathbf{k}\nu}\rangle = |\psi_{\mathbf{k}\nu}\rangle + \sum_{mn} q_{mn}^I |\beta_m^I\rangle \langle \beta_n^I | \psi_{\mathbf{k}\nu}\rangle, \quad (10)$$

where the coefficients q_{mn}^I are defined together with the pseudopotential.

2.2.1. Kinetic energy

The kinetic energy is calculated in reciprocal space. Using the Bloch theorem we write the Bloch wave-functions as:

$$\psi_{\mathbf{k}\nu}(\mathbf{r}) = e^{i\mathbf{k}\mathbf{r}} u_{\mathbf{k}\nu}(\mathbf{r}) = \frac{1}{\sqrt{V}} \sum_{\mathbf{G}} C_{\mathbf{k}+\mathbf{G}\nu} e^{i(\mathbf{k}+\mathbf{G})\mathbf{r}}, \quad (11)$$

where $u_{\mathbf{k}\nu}(\mathbf{r})$ is a lattice periodic function expanded in plane waves (here V is the volume of the solid) and the sum is over the reciprocal lattice vectors contained into a sphere defined by the relationship:

$$\frac{1}{2}|\mathbf{k} + \mathbf{G}|^2 < E_{cut}, \quad (12)$$

where E_{cut} is the kinetic energy cut-off. Then we have:

$$-\frac{1}{2}\nabla^2\psi_{\mathbf{k}\nu}(\mathbf{r}) = \frac{1}{\sqrt{V}} \sum_{\mathbf{G}} C'_{\mathbf{k}+\mathbf{G}\nu} e^{i(\mathbf{k}+\mathbf{G})\mathbf{r}}, \quad (13)$$

where:

$$C'_{\mathbf{k}+\mathbf{G}\nu} = \frac{1}{2}|\mathbf{k} + \mathbf{G}|^2 C_{\mathbf{k}+\mathbf{G}\nu}. \quad (14)$$

2.2.2. Local potential

The fast Fourier transform (FFT) transforms functions in real space into reciprocal space and the inverse FFT makes the inverse transformation.

From the coefficients $C_{\mathbf{k}+\mathbf{G}\nu}$, applying an inverse FFT we obtain the Bloch function in real space (up to a factor $1/\sqrt{V}$):

$$C_{\mathbf{k}+\mathbf{G}\nu} \xrightarrow{FFT^{-1}} u_{\mathbf{k}\nu}(\mathbf{r}) = \sum_{\mathbf{G}} C_{\mathbf{k}+\mathbf{G}\nu} e^{i\mathbf{G}\mathbf{r}}. \quad (15)$$

The effective potential is applied in real space as:

$$u'_{\mathbf{k}\nu}(\mathbf{r}) = V_{eff}(\mathbf{r})u_{\mathbf{k}\nu}(\mathbf{r}), \quad (16)$$

and a final FFT computes the plane wave expansion of $u'_{\mathbf{k}\nu}(\mathbf{r})$:

$$u'_{\mathbf{k}\nu}(\mathbf{r}) \xrightarrow{FFT} C'_{\mathbf{k}+\mathbf{G}\nu} = \frac{1}{N_{\mathbf{r}}} \sum_{\mathbf{r}} u'_{\mathbf{k}\nu}(\mathbf{r}) e^{-i\mathbf{G}\mathbf{r}}, \quad (17)$$

where $N_{\mathbf{r}}$ is the number of points of the FFT grid (see below).

The actual calculation of V_{eff} requires the calculation of the charge density in terms of the wave-functions $\psi_{\mathbf{k}\nu}$. However since we have not modified this part of the calculation we do not discuss it in detail. We assume only to have a function V_{eff} defined in the points of the FFT grid \mathbf{r} .

2.2.3. Non local pseudopotential and overlap matrix

The application of the non local potential needs three matrix-matrix multiplications:

$$\lambda_{n\mathbf{k}\nu}^I = \langle \beta_n^I | \psi_{\mathbf{k}\nu} \rangle = \sum_{\mathbf{G}} \beta_n^I(\mathbf{k} + \mathbf{G})^* C_{\mathbf{k}+\mathbf{G}\nu}, \quad (18)$$

$$\gamma_{m\mathbf{k}\nu}^I = \sum_n D_{mn}^I \lambda_{n\mathbf{k}\nu}^I, \quad (19)$$

$$V_{NL} |\psi_{\mathbf{k}\nu}\rangle = \sum_{Im} \gamma_{m\mathbf{k}\nu}^I |\beta_m^I\rangle. \quad (20)$$

Similarly, the application of the S matrix is:

$$\delta_{m\mathbf{k}\nu}^I = \sum_n q_{mn}^I \lambda_{n\mathbf{k}\nu}^I, \quad (21)$$

$$S |\psi_{\mathbf{k}\nu}\rangle = |\psi_{\mathbf{k}\nu}\rangle + \sum_{Im} \delta_{m\mathbf{k}\nu}^I |\beta_m^I\rangle. \quad (22)$$

where $\lambda_{n\mathbf{k}\nu}^I$ are those calculated in Eq. 18.

2.3. Density functional perturbation theory

The phonon frequencies and displacement modes are obtained by diagonalization of the dynamical matrix:

$$\omega_{\mathbf{q}}^2 \mathbf{u}_{s\alpha}(\mathbf{q}) = \sum_{s'\beta} D_{s\alpha s'\beta}(\mathbf{q}) \mathbf{u}_{s'\beta}(\mathbf{q}), \quad (23)$$

where $D_{s\alpha s'\beta}(\mathbf{q})$ is the dynamical matrix:

$$D_{s\alpha s'\beta}(\mathbf{q}) = \frac{1}{\sqrt{M_s M_{s'}}} \sum_{\nu} \frac{\partial^2 E_{tot}}{\partial \mathbf{u}_{\mu s\alpha} \partial \mathbf{u}_{\nu s'\beta}} e^{i\mathbf{q}(\mathbf{R}_{\nu} - \mathbf{R}_{\mu})}, \quad (24)$$

where E_{tot} is the DFT total energy, \mathbf{q} is a wave vector in the Brillouin zone (BZ), \mathbf{R}_{μ} are the Bravais lattice vectors, M_s are the atomic masses, and $\mathbf{u}_{\mu s\alpha}$ are the atomic displacements.

The second derivative of the DFT total energy can be written in terms of the change of the wave-functions due to a phonon perturbation projected on

the conduction band. These functions are the solutions of a linear system: [45, 46]

$$\left[H_{KS}^{\mathbf{k}+\mathbf{q}} + \alpha Q^{\mathbf{k}+\mathbf{q}} - \varepsilon_{\mathbf{k}\nu} S \right] P_c^{\mathbf{k}+\mathbf{q}} \frac{\partial u_{\mathbf{k}\nu}(\mathbf{r})}{\partial \mathbf{u}_{s'\beta}(\mathbf{q})} = -P_c^{\mathbf{k}+\mathbf{q}} \left[\frac{\partial V_{KS}}{\partial \mathbf{u}_{s'\beta}(\mathbf{q})} - \varepsilon_{\mathbf{k},\nu} \frac{\partial S}{\partial \mathbf{u}_{s'\beta}(\mathbf{q})} \right] u_{\mathbf{k}\nu}(\mathbf{r}), \quad (25)$$

where $P_c^{\mathbf{k}+\mathbf{q}}$ is the projector in the conduction band and $\frac{\partial V_{KS}}{\partial \mathbf{u}_{s'\beta}(\mathbf{q})} = \frac{\partial V_{loc}}{\partial \mathbf{u}_{s'\beta}(\mathbf{q})} + \frac{\partial V_H}{\partial \mathbf{u}_{s'\beta}(\mathbf{q})} + \frac{\partial V_{xc}}{\partial \mathbf{u}_{s'\beta}(\mathbf{q})} + \frac{\partial V_{NL}}{\partial \mathbf{u}_{s'\beta}(\mathbf{q})}$. The change of the Hartree and exchange and correlation potential are:

$$\begin{aligned} \frac{\partial V_H}{\partial \mathbf{u}_{s'\beta}(\mathbf{q})} &= \int \frac{e^{i\mathbf{q}(\mathbf{r}'-\mathbf{r})}}{|\mathbf{r}-\mathbf{r}'|} \frac{\partial \rho(\mathbf{r}')}{\partial \mathbf{u}_{s'\beta}(\mathbf{q})} d^3 r', \\ \frac{\partial V_{xc}}{\partial \mathbf{u}_{s'\beta}(\mathbf{q})} &= \frac{dV_{xc}}{d\rho} \frac{\partial \rho(\mathbf{r})}{\partial \mathbf{u}_{s'\beta}(\mathbf{q})}, \end{aligned} \quad (26)$$

and depend self-consistently on the charge density induced by the perturbation:

$$\frac{\partial \rho(\mathbf{r})}{\partial \mathbf{u}_{s'\beta}(\mathbf{q})} = 4 \sum_{\mathbf{k}\nu} \left[u_{\mathbf{k}\nu}^*(\mathbf{r}) P_c^{\mathbf{k}+\mathbf{q}} \frac{\partial u_{\mathbf{k}\nu}(\mathbf{r})}{\partial \mathbf{u}_{s'\beta}(\mathbf{q})} \right] + \Delta_{\mathbf{u}_{s'\beta}(\mathbf{q})}(\mathbf{r}), \quad (27)$$

where the last term represents the change of the augmentation charge calculated in the ultrasoft and PAW case but not accelerated in the present work. [46] $Q^{\mathbf{k}+\mathbf{q}}$ is a projection in the valence manifold, [45] while the change of the nonlocal pseudopotential is described in more detail in the given references (see for instance Ref. [46]).

$\alpha Q^{\mathbf{k}+\mathbf{q}}$ can be written in the form:

$$\alpha Q^{\mathbf{k}+\mathbf{q}} = \alpha \sum_{\mu} S |u_{\mathbf{k}+\mathbf{q}\mu}\rangle \langle u_{\mathbf{k}+\mathbf{q}\mu}| S, \quad (28)$$

and its application to a set of wave functions $|x_{\mathbf{k}+\mathbf{q}\nu j}\rangle$ (here j indicates the different perturbations $s'\beta$) can be calculated easily using the fact that $S|x_{\mathbf{k}+\mathbf{q}\nu j}\rangle$ is already known from the routine that applies $H_{KS}^{\mathbf{k}+\mathbf{q}}$ and S . We have a first matrix-matrix multiplication:

$$\mu_{\mathbf{k}+\mathbf{q}j\nu} = \langle u_{\mathbf{k}+\mathbf{q}\mu}| S |x_{\mathbf{k}+\mathbf{q}\nu j}\rangle \alpha, \quad (29)$$

then a second one:

$$|y_{\mathbf{k}+\mathbf{q}\nu j}\rangle = \sum_{\mu} |u_{\mathbf{k}+\mathbf{q}\mu}\rangle \mu_{\mathbf{k}+\mathbf{q}j\mu\nu}, \quad (30)$$

and finally we must apply S to the vectors $|y_{\mathbf{k}+\mathbf{q}\nu j}\rangle$ and we have:

$$\alpha Q^{\mathbf{k}+\mathbf{q}} |x_{\mathbf{k}+\mathbf{q}\nu j}\rangle = S |y_{\mathbf{k}+\mathbf{q}\nu j}\rangle = |y_{\mathbf{k}+\mathbf{q}\nu j}\rangle + \sum_{Imn} q_{mn}^I |\beta_m^I\rangle \langle \beta_n^I | y_{\mathbf{k}+\mathbf{q}\nu j}\rangle, \quad (31)$$

and this requires other three matrix-matrix multiplications as illustrated above.

The self-consistent linear system (Eq. 25) is solved by iterations. From an initial guess of the potentials, of $\frac{\partial V_H}{\partial \mathbf{u}_{s'\beta}(\mathbf{q})} + \frac{\partial V_{xc}}{\partial \mathbf{u}_{s'\beta}(\mathbf{q})}$, the linear system is solved and new induced charge and potentials are obtained. Mixing the latter with the potentials used in the linear system it is possible to reach a self-consistent solution.

The most time consuming step of this process is however the solution of the linear system at fixed $\frac{\partial V_H}{\partial \mathbf{u}_{s'\beta}(\mathbf{q})} + \frac{\partial V_{xc}}{\partial \mathbf{u}_{s'\beta}(\mathbf{q})}$ so we will focus on this step.

2.4. Preconditioned conjugate gradient

The algorithm used for the solution of Eq. 25 with a given right hand side is a preconditioned conjugate-gradient iterative algorithm. [47, 48, 49] Given a starting guess x of the solution of the problem $Ax = b$, we improve it with the following algorithm:

$$r \leftarrow Ax - b, \quad (32)$$

$$d \leftarrow M^{-1}r, \quad (33)$$

$$\rho \leftarrow d^T r, \quad (34)$$

$$\gamma \leftarrow \frac{\rho}{\rho_{old}}, \quad (35)$$

$$d \leftarrow d + \gamma d_{old}, \quad (36)$$

$$t \leftarrow Ad, \quad (37)$$

$$\lambda \leftarrow -\frac{d^T r}{d^T t}, \quad (38)$$

$$x \leftarrow x + \lambda d, \quad (39)$$

$$r \leftarrow r + \lambda t, \quad (40)$$

$$d_{old} \leftarrow d, \quad (41)$$

$$\rho_{old} \leftarrow \rho, \quad (42)$$

and iterate from Eq. 33 until the modulus of ρ is smaller than an input threshold. Here the arrows indicate that the variables on the left are substituted with those on the right. r is the negative of the residual vector while d contains minus the preconditioned residual in Eqs. 33 to 36 and minus the search direction from Eq. 36. Eqs. 35 and 36 are executed only from the second iteration onwards. The algorithm requires memory sufficient to save the vectors r , d , t , d_{old} of the same size of the input vector x . ρ and ρ_{old} , as well as γ and λ , are instead scalars. Moreover, we need two external routines to apply A and M^{-1} . The most time consuming step is the application of the matrix A to d . In our case $A = H_{KS}^{\mathbf{k}+\mathbf{q}} + \alpha Q^{\mathbf{k}+\mathbf{q}} - \varepsilon_{\mathbf{k}\nu} S$ so again the acceleration rests on the routine that applies $H_{KS}^{\mathbf{k}+\mathbf{q}}$ and S described above. For the preconditioning the following matrix diagonal in reciprocal space $M_{\mathbf{G},\mathbf{G}} = MAX(1.0, \frac{|\mathbf{k}+\mathbf{q}+\mathbf{G}|^2}{2\langle\psi_{\mathbf{k}+\mathbf{q}\nu}|\frac{1}{2}\nabla^2|\psi_{\mathbf{k}+\mathbf{q}\nu}\rangle})$ is used and this vector is passed to the routine. The conjugate gradient algorithm is applied to each \mathbf{k} point and to each N_{pe} perturbations. The N_b bands of a given \mathbf{k} point are optimized together but the different \mathbf{k} points and different perturbations are treated in sequence, one after the other. Only one \mathbf{q} is calculated in each run. This algorithm has been used in the last thirty years in Quantum ESPRESSO to solve the linear system. Similar algorithms, with appropriate modifications, can be used also to minimize the total energy and solve the Kohn and Sham equations. [50]

3. GPU optimization

Quantum ESPRESSO has several levels of parallelization on the CPU. It is possible to divide the \mathbf{k} -points in groups (called `pools`) and assign each group to a set of cores. These cores may be further divided in groups, with each group dealing with a set of bands (`bands` parallelization) and finally each group of cores dealing with a set of bands can further divide the reciprocal lattice vectors (\mathbf{G}) and work only on a subset of these (`\mathbf{G} vectors` parallelization). It is at this point that one can introduce the GPU acceleration. The standard method to use the GPU consists into allocating variables on the device memory (the GPU) and to call from `HOST` routines developed by `Nvidia` that perform linear algebra (`cuBLAS`) operations or `FFTs` (`cuFFT`) on the data allocated on the device. It is also possible to add compiler directives to run loops in parallel on the GPU without changing the code.

The standard Davidson algorithm works sequentially on each \mathbf{k} point of a `pool` and solves for all the bands (calling the routines that apply H_{KS}

Figure 1: Algorithms used in the standard approach and in our optimized GPU approach for the diagonalization of the Hamiltonian.

Algorithm 1 CPU and standard GPU diagonalization

```

for ik = 1, nks do                                     ▷ nks = #k points per pool
    build  $H_{KS}^k$  and  $S^k$ 
    compute  $\varepsilon_{k\nu}$  and  $\psi_{k\nu}$  by Davidson ( $N_b$ )
end for

```

Algorithm 2 Optimized GPU diagonalization

```

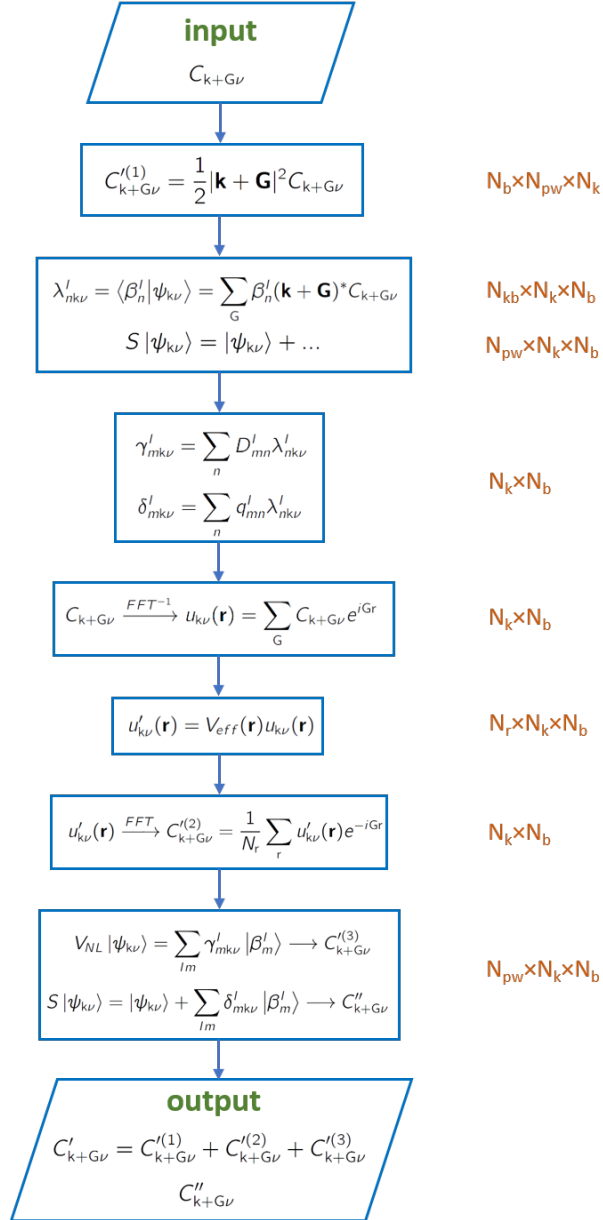
for ikb = 1, nkbblock do                               ▷ nkbblock = #k points blocks
    build in parallel  $H_{KS}^k$  and  $S^k$  on GPU threads ( $N_k$ )
    compute  $\varepsilon_{k\nu}$  and  $\psi_{k\nu}$  by Davidson on GPU threads ( $N_b \times N_k$ )
end for

```

and S for a subset of bands, if `bands` parallelization is used). Therefore the number of times in which the GPU memory is loaded increases linearly with the number of \mathbf{k} points. When the size of the problem is small, it can happen that the library matrix-matrix multiplications and FFTs routines cannot exploit all the capacity of the GPU because they have too few data to work on. As a result a GPU calculation might become even slower than a CPUs only calculation. Parallelizing on the \mathbf{G} vectors just reduces further the size of the data allocated on the GPU for each \mathbf{k} point and does not help in this case. Moreover, presently the GPU acceleration does not work well if many CPUs use the same GPU, so we use as many CPUs as GPUs.

Our strategy for accelerating the code on the GPU is illustrated schematically in Fig. 1. We put on the GPU memory as many wave-functions (i.e. \mathbf{k} points) as possible in a block of N_k \mathbf{k} points and run simultaneously on all these \mathbf{k} points the operations of the Davidson algorithm needed to diagonalize the Hamiltonian. Each `pool` of CPUs cores works on its set of \mathbf{k} points as assigned by the `pool` parallelization of `Quantum ESPRESSO` and only these \mathbf{k} points are divided in blocks for the GPU acceleration. `Bands` parallelization and \mathbf{G} vector parallelization presently are not supported by our approach. The main GPU optimization has been performed on the routine that applies H_{KS} and S to the wave-functions $\psi_{k\nu}$, but some acceleration has been obtained also carrying out the operations of the Davidson algorithm in parallel on many \mathbf{k} points. In our approach, the routine that applies H_{KS} and S is a `HOST` routine (i.e. a routine running on the CPU) that receives as input

Figure 2: Flowchart of the routine that applies $H_{KS}^{\mathbf{k}}$ and $S^{\mathbf{k}}$ to the wavefunctions. Close to each routine we write the number of threads that are used to run it on the GPU.



$C_{\mathbf{k}+\mathbf{G}\nu}$ for N_k \mathbf{k} points, and gives as output the coefficients $C'_{\mathbf{k}+\mathbf{G}\nu}$ and $C''_{\mathbf{k}+\mathbf{G}\nu}$ of the plane waves expansion of $H_{KS}\psi_{\mathbf{k}\nu}$ and of $S\psi_{\mathbf{k}\nu}$. This routine calls in sequence several **GLOBAL** routines (that is routines that run on the GPU and for which we can specify how many GPU threads run in parallel). The sequence of routines and the formula that they implement is illustrated in Fig. 2. The first computes the kinetic energy and runs $N_{pw} \times N_k \times N_b$ threads each one dealing with a \mathbf{G} vector of one \mathbf{k} point and of one band (here N_{pw} is the number of \mathbf{G} vectors used to expand the wave-functions). A second routine computes the scalar product in Eq. 18 and runs $N_{kb} \times N_k \times N_b$ threads, where N_{kb} is the total number of projectors $|\beta_m^I\rangle$. The latter are loaded on the GPU for all the N_k points before calling the Davidson algorithm. Another **GLOBAL** routine computes Eqs. 19 and 21 and runs $N_k \times N_b$ threads, while the sum over n is made inside the routine. A routine copies $C_{\mathbf{k}+\mathbf{G}\nu}$ in $C''_{\mathbf{k}+\mathbf{G}\nu}$ and this is made in parallel running $N_{pw} \times N_k \times N_b$ threads. This is the first term of the application of S to the wave functions. A routine sets to zero the FFT grid running $N_r \times N_k \times N_b$ threads and another one sets the non zero elements of this grid running $N_k \times N_b$ threads, each one dealing with all the N_r grid points for one \mathbf{k} point and one band. Then a set of three routines applies an inverse FFT to the wave-functions as detailed below, and a routine applies V_{eff} running $N_r \times N_k \times N_b$ threads. Another set of three routines applies the FFT to return to reciprocal space and a routine collects the results from the grid and adds them to $C'_{\mathbf{k}+\mathbf{G}\nu}$. This is made in parallel on the GPU running $N_k \times N_b$ threads. Finally Eq. 20 is calculated by a routine that runs $N_{pw} \times N_k \times N_b$ threads and adds the result to $C'_{\mathbf{k}+\mathbf{G}\nu}$. In the ultrasoft or PAW PPs case, the same routine calculates also the second term in the right hand side of Eq. 22 and adds it to $C''_{\mathbf{k}+\mathbf{G}\nu}$.

In this algorithm, N_k must be carefully chosen and depends on the amount of GPU memory and on the size of the FFT grid. N_k is mainly limited by the necessity to allocate on the GPU $N_k \times N_b$ FFT grids to apply, in parallel, the local potential to the Bloch functions. The allocation of this memory is done by the **HOST** routine that implements the Davidson algorithm.

We have also optimized some parts of the Davidson algorithm. The standard routine has been generalized introducing several loops on the N_k \mathbf{k} points and part of these loops have been transformed into kernel routines (**GLOBAL** routines) that perform the calculation in parallel using $N_k \times N_b$ threads. We have accelerated only the loops that took a significant amount of time. The other loops call the linear algebra **cuBlas** routines as in the standard approach.

Figure 3: Algorithms used in the standard phonon code and in our optimized GPU approach for solving the linear system that gives the perturbed wavefunctions.

Algorithm 3 CPU and standard GPU phonon algorithm

```

for ik = 1, nks do
  build  $H_{KS}^{\mathbf{k}+\mathbf{q}}$  and  $S^{\mathbf{k}+\mathbf{q}}$ 
  for ipert = 1, npe do ▷ npe = #perturbations
    build  $P_c^{\mathbf{k}+\mathbf{q}} \frac{\partial V_{KS}}{\partial u_{s\alpha}(\mathbf{q})} u_{\mathbf{k}\nu}$  ( $N_b$ )
    compute  $\frac{\partial u_{\mathbf{k}\nu}}{\partial u_{s\alpha}(\mathbf{q})}$  by conjugate gradient (CG) ( $N_b$ )
  end for
end for

```

Algorithm 4 Optimized GPU phonon algorithm

```

for ikb = 1, nkbblock do ▷  $N_k$  = #k points per block
  build in parallel  $H_{KS}^{\mathbf{k}+\mathbf{q}}$  and  $S^{\mathbf{k}+\mathbf{q}}$  on GPU threads ( $N_k$ )
  build in parallel  $P_c^{\mathbf{k}+\mathbf{q}} \frac{\partial V_{KS}}{\partial u_{s\alpha}(\mathbf{q})} u_{\mathbf{k}\nu}$  on GPU threads ( $N_b \times N_k \times N_{pe}$ )
  compute  $\frac{\partial u_{\mathbf{k}\nu}}{\partial u_{s\alpha}(\mathbf{q})}$  by CG on GPU threads ( $N_b \times N_k \times N_{pe}$ )
end for

```

The acceleration of the phonon code instead has been carried out essentially on the algorithm that solves the linear system in Eq. 25. We proceed as in the Davidson algorithm (see the scheme in Fig. 3). However, in the phonon case the calculation of the induced charge density (Eq. 27) requires two FFT grids per band, one to contain $u_{\mathbf{k}\nu}^*(\mathbf{r})$ and one to contain $P_c^{\mathbf{k}+\mathbf{q}} \frac{\partial u_{\mathbf{k}\nu}(\mathbf{r})}{\partial \mathbf{u}_{s'\beta}(\mathbf{q})}$ so usually we use N_k smaller than in the Davidson algorithm. The GPU optimization of the preconditioned conjugate gradient algorithm starts by allocating the COMPLEX vectors g , d , d_{old} , and t on the GPU. For each variable $N_k \times N_b \times N_{pe}$ arrays are allocated. This memory is much larger than the one of the standard algorithm that requires only N_b copies of each variable, but this space is allocated only on the GPU. The algorithm is then divided in loops over the N_k \mathbf{k} points, the N_{pe} perturbations, and the N_b bands. Loop one executes Eqs. 33 and Eqs. 34, loop two executes Eq. 36, and loop three computes $d^T r$ and $d^T t$ that appear in the numerator and denominator of Eq. 38. Finally loop four computes Eqs. 39, 40, and 41. Each loop is transformed into routine with the GLOBAL attribute that runs $N_k \times N_b \times N_{pe}$ threads, each one computing one perturbation to one band of one \mathbf{k} point. Since each thread

executes only a scalar product or an operation of the type $x \leftarrow x + \lambda d$ we have programmed these routines in `CUDA Fortran` without calling any other library routine. The array themselves instead are not split and each thread works on all the \mathbf{G} vectors of each wave-function. All the other steps of the algorithm involve only scalar operations that are performed by the CPU.

Eq. 32 and Eq. 37 require an external routine to apply A to the vectors x (or d). For this operator we use the same routine that applies H_{KS} and S in the Davidson algorithm. The routine works in general for an arbitrary number of wavefunctions so when called from the conjugate gradient algorithm, in parallel on the GPU threads, it deals with the $N_k \times N_{pe}$ set of wavefunctions, each one composed by N_b bands. We have then written a `HOST` routine that receives as input the coefficients $C'_{\mathbf{k}+\mathbf{q}\nu j}$ and $C''_{\mathbf{k}+\mathbf{q}\nu j}$ of the Fourier transform of $H_{KS}^{\mathbf{k}+\mathbf{q}}|x_{\mathbf{k}+\mathbf{q}\nu j}\rangle$ and $S|x_{\mathbf{k}+\mathbf{q}\nu j}\rangle$ and gives as output the Fourier coefficients of $A|x_{\mathbf{k}+\mathbf{q}\nu j}\rangle$. This routine calls a series of `GLOBAL` routines for which we can control the number GPU threads that run in parallel. The first routine computes Eq. 29 and runs $N_k \times N_{pe} \times N_b \times N_b$ threads. A second routine computes $|a_{\mathbf{k}+\mathbf{q}\nu j}\rangle = H_{KS}^{\mathbf{k}+\mathbf{q}}|x_{\mathbf{k}+\mathbf{q}\nu j}\rangle - \varepsilon_{\mathbf{k}\nu}S|x_{\mathbf{k}+\mathbf{q}\nu j}\rangle$ and runs $N_k \times N_{pe} \times N_b$ threads. To complete the operator A we have to calculate the operator $\alpha Q^{\mathbf{k}+\mathbf{q}}|x_{\mathbf{k}+\mathbf{q}\nu j}\rangle$ and we optimized also this part to run in many threads on the GPU in parallel on the \mathbf{k} vectors, the bands, and the perturbations. This is done by calling another set of `GLOBAL` routines. The first computes Eq. 30 running on $N_k \times N_{pe} \times N_b$ threads, another one computes the scalar products $\langle \beta_n^I | y_{\mathbf{k}+\mathbf{q}\nu j} \rangle$ that appear in Eq. 31 and runs $N_k \times N_{pe} \times N_{kb} \times N_b$ threads, and a third routine calculates Eq. 21 using the scalar products just calculated and runs on $N_k \times N_{pe} \times N_b$ threads. Finally a `GLOBAL` routine computes Eq. 31 and adds it to $|a_{\mathbf{k}+\mathbf{q}\nu j}\rangle$ running in $N_k \times N_{pe} \times N_b \times N_{pw}$ threads.

4. Fast Fourier transform

The application of $V_{eff}(\mathbf{r})$ to one Bloch wave-function requires two Fourier transforms. It is convenient to introduce a mesh in reciprocal space:

$$\mathbf{G}_{m_1, m_2, m_3} \equiv m_1 \mathbf{b}_1 + m_2 \mathbf{b}_2 + m_3 \mathbf{b}_3, \quad (43)$$

where \mathbf{b}_1 , \mathbf{b}_2 , and \mathbf{b}_3 are the principal reciprocal lattice vectors and m_1 , m_2 , and m_3 are integers, and a mesh in real space:

$$\mathbf{r}_{l_1, l_2, l_3} = \frac{l_1}{N_1} \mathbf{a}_1 + \frac{l_2}{N_2} \mathbf{a}_2 + \frac{l_3}{N_3} \mathbf{a}_3, \quad (44)$$

where \mathbf{a}_1 , \mathbf{a}_2 , and \mathbf{a}_3 are the direct lattice vectors, and l_1 , l_2 , and l_3 are integers. The integers N_1 , N_2 , and N_3 define the size of the mesh in real space and, equivalently, the size of the mesh in reciprocal space. They must be sufficiently large so that the vectors $\mathbf{G}_{m_1, m_2, m_3}$ contain all the vectors $\mathbf{G} - \mathbf{G}'$ defined by the basis set.

Given a function in reciprocal space, defined on the \mathbf{G} vectors $\tilde{f}(m_1, m_2, m_3) \equiv f(\mathbf{G}_{m_1, m_2, m_3})$, its real space form $f(l_1, l_2, l_3) = f(\mathbf{r}_{l_1, l_2, l_3})$ is given by:

$$f(l_1, l_2, l_3) = \sum_{m_1=0}^{N_1-1} \sum_{m_2=0}^{N_2-1} \sum_{m_3=0}^{N_3-1} \tilde{f}(m_1, m_2, m_3) e^{i2\pi l_1 m_1 / N_1} e^{i2\pi l_2 m_2 / N_2} e^{i2\pi l_3 m_3 / N_3}. \quad (45)$$

The transform is made in three steps. In the first step, we compute $N_1 \times N_2$ one dimensional FFTs along z :

$$\bar{f}(m_1, m_2, l_3) = \sum_{m_3=0}^{N_3-1} \tilde{f}(m_1, m_2, m_3) e^{i2\pi l_3 m_3 / N_3}. \quad (46)$$

We run $N_1 \times N_b \times N_k$ threads on the GPU by calling a GLOBAL routine, and each thread computes N_2 FFTs. Each FFT (sum over m_3) is carried out by calling an FFT library routine (`cffft1b` from `fftpack.5.1`) which is declared as a DEVICE routine. In the second step, we compute:

$$\hat{f}(m_1, l_2, l_3) = \sum_{m_2=0}^{N_2-1} \bar{f}(m_1, m_2, l_3) e^{i2\pi l_2 m_2 / N_2}. \quad (47)$$

In this case we run $N_1 \times N_b \times N_k$ threads each one doing N_3 FFTs. Each FFT (sum over m_2) is carried out by the DEVICE FFT library routine `cffft1b`. Finally, to complete the three dimensional Fourier transform, in the third step we calculate:

$$f(l_1, l_2, l_3) = \sum_{m_1=0}^{N_1-1} \hat{f}(m_1, l_2, l_3) e^{i2\pi l_1 m_1 / N_1}. \quad (48)$$

In this case we run $N_k \times N_b$ threads on the GPU each one computing $N_2 \times N_3$ FFTs. Each one dimensional FFT (sum over m_1) is carried out by the DEVICE FFT library routine `cffft1b`. In a similar way one can make a three

dimensional Fourier transform to obtain the reciprocal space function from its real space form:

$$\tilde{f}(m_1, m_2, m_3) = \frac{1}{N_{\mathbf{r}}} \sum_{l_1=0}^{N_1-1} \sum_{l_2=0}^{N_2-1} \sum_{l_3=0}^{N_3-1} f(l_1, l_2, l_3) e^{-i2\pi l_1 m_1 / N_1} e^{-i2\pi l_2 m_2 / N_2} e^{-i2\pi l_3 m_3 / N_3}, \quad (49)$$

where $N_{\mathbf{r}} = N_1 N_2 N_3$. In this case we call the `DEVICE` function `cfft1f` to actually carry out the one dimensional FFTs.

The product of V_{eff} with the wave-function:

$$u'_{\mathbf{k}\nu}(l_1, l_2, l_3) = V_{eff}(l_1, l_2, l_3) u_{\mathbf{k}\nu}(l_1, l_2, l_3), \quad (50)$$

is made by running $N_{\mathbf{r}} \times N_k \times N_b$ threads on the GPU, each thread computing one product. After computing the product, an FFT as in Eq. 49 gives the Fourier components of the product that can be added to those obtained by applying the kinetic energy. This FFT is performed by three routines similar to those described for the inverse FFT.

4.1. FFT on the device

Eqs. 46,47,48 cannot be implemented as written since they involve N_i^2 operations, where N_i is N_1 , N_2 or N_3 . These sums can be done more efficiently with an FFT algorithm that requires $N_i \log(N_i)$ operations. [47] The `FFTXlib` of Quantum ESPRESSO contains both the three dimensional FFT driver and a copy of an old FFTW library. [51] It also supports the newer FFTW3 library, some vendor-specific FFT libraries, and it can call library routines optimized for the GPU in cuFFT [9, 20]. Moreover, it can carry out the FFT in parallel when the FFT mesh (and \mathbf{G} vectors) are distributed among different MPI processes. However, these routines are called from the CPU HOST with actual argument variables that are allocated on the GPU and they take care of launching the kernel threads on the GPU. In our approach, the FFT routines are called from inside the GPU threads and therefore must have the `DEVICE` attribute, hence `FFTXlib` cannot be used. The library that offers this functionality `cuFFTDx` is written in C++ and it has not yet a FORTRAN interface. Therefore, we have taken the `fftpack5.1` [52] which is distributed under the GNU GPL licence together with its Fortran source and we have modified each routine and function of this library by adding the `ATTRIBUTES(DEVICE)`. We have also constructed a Fortran interface for each routine so that the routines that

include the interface can know that the routines of `fftpack` are actually `DEVICE` routines and accept variables allocated on the `GPU`. The modified library is distributed together with the `thermo_pw` package.

5. Matrix Diagonalization

The Davidson algorithm requires the solution of a generalized eigenvalue problem in a reduced basis:

$$Ax = \lambda Bx, \tag{51}$$

where A and B are Hermitian matrices and λ and x are the eigenvalues and eigenvectors. Usually, the `CPU` makes this calculation by calling `LAPACK` routines [43] such as `ZHEGVX` that computes selected eigenvalues and, optionally, eigenvectors of a complex generalized Hermitian-definite eigenproblem, or `ZHEGV` that computes all eigenvalues and eigenvectors of the same matrices. It is also possible to call library routines optimized for the `GPU` of the `cuSolver` or of the `MAGMA` libraries. A `HOST` driver that calls these routines is contained in the `LAXlib` library distributed with `Quantum ESPRESSO`. We have tested this approach creating a loop over the N_k \mathbf{k} points that calls these routines, but found that it is possible to obtain a significant speed up by simultaneously diagonalizing the generalized eigenvalue problem for many \mathbf{k} points. We run therefore a `GLOBAL` routine with as many threads as possible (ideally N_k , but see below). In order to solve the generalized eigenvalue problem inside a `GLOBAL` routine we cannot call `HOST` routines such as those available in `cuSolver` or in `MAGMA` [21] what is needed is a library that can be called from inside the `GPU` threads (with `DEVICE` routines). Since we are not aware of any `DEVICE` implementation of `LAPACK`, we took the routines `ZHEGVX` and `ZHEGV` together with those called by them, transformed them into `DEVICE` routines, and wrote the corresponding `Fortran` interfaces. We found only one problem with this approach: The routine `ZPOTRF2`, which performs the Cholesky factorization of a Hermitian positive definite matrix A , is recursive. Since `CUDA Fortran` does not allow for recursive `DEVICE` routines or functions, we rewrote it with a non recursive algorithm.

The number of \mathbf{k} points that can be diagonalized simultaneously is usually lower than N_k since the `LAPACK` `DEVICE` routines use a certain amount of `GPU` resources. So we divided the N_k \mathbf{k} points in blocks of maximum size determined empirically on the available machine.

6. Results

6.1. Benchmark Example

We have implemented our approach in the `thermo_pw` code [53] which is a driver of `Quantum ESPRESSO` routines to calculate materials properties. To activate the new approach, it suffices to set the flag `many_k` to `.TRUE.` and the input variable `memgpu` to the amount of GPU memory (in GBytes). Both variables are written in the `thermo_control` input file. The new routines are in the directory `qe` of `thermo_pw`, while the `LAPACK` and `fftpack5.1` routines modified with the `ATTRIBUTES(DEVICE)` together with their interfaces are distributed in separate subdirectories of the `thermo_pw` package. For further details please refer to the `thermo_pw` user’s guide.

Our benchmark is a part of the calculations carried out to compute the quasi-harmonic temperature dependent elastic constants of tungsten. [29] Our system is body centered cubic (bcc) tungsten simulated with the PBEsol exchange and correlation functional [54] at the lattice constant $a = 5.965$ a.u.. Tungsten is described with a PAW pseudopotential that has 14 valence electrons and we compute $N_b = 11$ bands. [55] We use cut-offs for the wave-functions/charge density of 90/360 Ry, a \mathbf{k} -point mesh of $45 \times 45 \times 45$ and deal with the Fermi surface with the smearing approach ([28]) with a smearing parameter $\sigma = 0.02$ Ry. The FFT mesh has size $32 \times 32 \times 32$ for a total of $N_r = 32768$ mesh points. We compute the phonon frequencies for the point $\mathbf{q} = \frac{2\pi}{a}(-1/8, -1/4, 3/8)$. The small space group of this \mathbf{q} point has no rotational symmetry in it, so we need to use the complete mesh of $45^3 = 91125$ \mathbf{k} points when computing the perturbed wave-functions. Since we need also the eigenvalues and eigenfunctions at $\mathbf{k} + \mathbf{q}$ we compute the band structure of 182250 \mathbf{k} points.

We report the time obtained with `version 7.3` of `Quantum ESPRESSO` together with `thermo_pw version 2.0.0`. All tests have been performed on the `Leonardo` supercomputer at `CINECA`. Each node of the machine has a CPU with 32 cores and 4 Ampère GPUs. In the `Leonardo` manual, the theoretically declared peak performance of one node (32 cores) is 1680 Gflops while the four GPUs of one node can provide 75000 Gflops. There is therefore a maximum theoretical acceleration of a factor of 45. We run on the GPUs using as many CPU cores as GPUs and each CPU runs one MPI process. [56] MPI processes can communicate among themselves with MPI library calls. Each MPI process communicates with one GPU, multiple MPI processes using the same GPU are not allowed. Moreover we do not use direct GPU-GPU communication. When

several MPI processes run, the total number of \mathbf{k} points is divided in a number of pools equal to the number of MPI processes. The code is compiled with the PGI Fortran compiler contained in the Nvidia SDK [57].

6.2. FFT

Table 1: Comparison of the time spent by computing the FFT and the inverse FFT when applying the Hamiltonian operator in the Davidson algorithm and in the conjugate gradient algorithm for the example described in the paper.

| | CPU | | | | | GPU | | | | optimized GPU | | | |
|-----------|------|------|------|------|------|-------|------|------|------|---------------|------|------|-----|
| #CPU | 32 | 32 | 32 | 64 | 64 | 1 | 2 | 4 | 8 | 1 | 2 | 4 | 8 |
| #GPU | 0 | 0 | 0 | 0 | 0 | 1 | 2 | 4 | 8 | 1 | 2 | 4 | 8 |
| #task(np) | 32 | 32 | 32 | 64 | 64 | 1 | 2 | 4 | 8 | 1 | 2 | 4 | 8 |
| #pool(nk) | 8 | 16 | 32 | 32 | 64 | 1 | 2 | 4 | 8 | 1 | 2 | 4 | 8 |
| time (s) | 6771 | 6280 | 4539 | 3269 | 2213 | 13415 | 6866 | 3441 | 1744 | 7532 | 3574 | 2068 | 934 |

In Table 1, we report the time necessary to compute the FFTs to apply the local potential. We consider three cases: CPUs only, standard GPU code that calls the cuFFT library, and the optimized GPU code that uses the `fftpack.5.1` routines declared as DEVICE routines. In the GPUs runs, we consider 1, 2, 4 or 8 GPUs. For the CPUs only runs, we use all the CPUs of one (32) or two nodes (64). Further, with 32 cores, the \mathbf{k} points are divided into 8, 16, or 32 pools, with 64 cores, into 32 or 64 pools. When comparing CPUs and GPUs, we compare 4 or 8 GPUs with the best times obtained with 32 or 64 cores, respectively. We start by discussing the CPUs only case. With both 32 or 64 cores, the minimum FFT time is obtained when the number of pools is equal to the number of cores. This indicates that in this system it is not useful to divide the \mathbf{G} vectors among CPUs. The second observation is that when we pass from one to two nodes the time halves, showing a good scaling with the number of nodes. We call T_{cpu} the best time obtained with one or two nodes. Passing now to the GPU times, we see that both with the standard algorithm and with the optimized one the computational time is inversely proportional to the number of GPUs. Comparing now the time taken by the standard GPU algorithm, we see that it is $0.76 T_{cpu}$ (4 GPUs), $0.79 T_{cpu}$ (8 GPUs). So, as far as the FFT is concerned, it is convenient to use the GPUs instead of the CPUs although the gain is not big. The optimized GPU algorithm gives times that are $0.46 T_{cpu}$ (4 GPU), $0.42 T_{cpu}$ (8 GPUs). This is much less than the theoretical capacity of the GPU, but still it makes

convenient to use the latter. When computing the FFT, the optimized GPU algorithm is 1.9 times faster (8 GPUs) than the standard GPU version that calls the CuFFT routines in sequence on the \mathbf{k} points.

6.3. Diagonalization

Table 2: Comparison of the time spent to diagonalize the reduced Hamiltonian using linear algebra routines (within the Davidson algorithm).

| | CPU | | | | | GPU | | | | optimized GPU | | | |
|-----------|-----|----|----|----|----|------|-----|-----|-----|---------------|-----|----|----|
| #CPU | 32 | 32 | 32 | 64 | 64 | 1 | 2 | 4 | 8 | 1 | 2 | 4 | 8 |
| #GPU | 0 | 0 | 0 | 0 | 0 | 1 | 2 | 4 | 8 | 1 | 2 | 4 | 8 |
| #task(np) | 32 | 32 | 32 | 64 | 64 | 1 | 2 | 4 | 8 | 1 | 2 | 4 | 8 |
| #pool(nk) | 8 | 16 | 32 | 32 | 64 | 1 | 2 | 4 | 8 | 1 | 2 | 4 | 8 |
| time (s) | 81 | 44 | 20 | 21 | 10 | 1286 | 684 | 348 | 178 | 220 | 118 | 60 | 29 |

In Table 2, we report the time spent by the diagonalization of the reduced Hamiltonian carried out by the LAPACK routines on the CPU, by the cuSolver library running on GPU called by the LAXlib package, and by the optimized GPU version of the code in which the Hamiltonians of many \mathbf{k} -vectors are diagonalized simultaneously by the LAPACK routines declared as DEVICE routines. The effect of using pools and several CPUs is also illustrated. The sizes of the matrices to be diagonalized vary, depending on the instantaneous size of the basis set in the Davidson algorithm. The routine must find the lowest $N_b = 11$ eigenpairs in a matrix that can have a maximum size equal to $4N_b = 44$. This is repeated for all \mathbf{k} points for all Davidson iterations and all self-consistent iterations in addition to a band structure calculation before the phonon calculation (in which there are about 2×10^5 \mathbf{k} points). The CPU diagonalization time scales linearly with the number of \mathbf{k} points and therefore depends only on the number of pools. Using 64 or 32 cores gives exactly the same time when we use 32 pools, but if we use a number of pools equal to the number of cores with two nodes we halves the diagonalization time with respect to one node. A good scaling is also shown by the GPU calculation. Increasing the number of GPUs increases the number of pools and therefore decreases the number of \mathbf{k} points per pool. With both the standard GPU algorithm and with the optimized one we could not run faster than the CPU. With the standard algorithm the size of the matrix to diagonalize is so small that the time to initialize the GPU greatly exceeds the CPU diagonalization time. In this particular example, the time of the standard GPU calculation is

$18 T_{cpu}$. With our optimization we could reduce this time to $3T_{cpu}$. In our example however the total time for the diagonalization is small with respect to all other times and we have not tried to further optimize this part.

6.4. Application of the Hamiltonian and of S

Table 3: Comparison of the total time spent to apply H_{KS} and S to the wave-functions in the Davidson algorithm and in the conjugate gradient algorithm.

| | CPU | | | | | GPU | | | | optimized GPU | | | |
|-------------------------------|------|------|------|------|------|-------|-------|------|------|---------------|------|------|------|
| | | | | | | | | | | | | | |
| #CPU | 32 | 32 | 32 | 64 | 64 | 1 | 2 | 4 | 8 | 1 | 2 | 4 | 8 |
| #GPU | 0 | 0 | 0 | 0 | 0 | 1 | 2 | 4 | 8 | 1 | 2 | 4 | 8 |
| #task(np) | 32 | 32 | 32 | 64 | 64 | 1 | 2 | 4 | 8 | 1 | 2 | 4 | 8 |
| #pool(nk) | 8 | 16 | 32 | 32 | 64 | 1 | 2 | 4 | 8 | 1 | 2 | 4 | 8 |
| time (s) | 7907 | 7319 | 5519 | 3780 | 2702 | 36157 | 18465 | 9263 | 4694 | 9138 | 4375 | 2472 | 1138 |
| time -time _{FFT} (s) | 1136 | 1039 | 980 | 511 | 489 | 22742 | 11599 | 5822 | 2950 | 1606 | 801 | 404 | 204 |

In Table 3 we show the time required for the application of the Hamiltonian and of the overlap matrix S to the wave-functions. This time comprises the time needed to apply the FFT and inverse FFT to the wave-functions, the time needed to apply the kinetic energy and the nonlocal pseudopotential as well as the time needed to apply the overlap matrix S . In the same table we report also the difference between these times and the times needed to carry out the FFT reported in Table 1. In the time reported in the table, we apply the operator H_{KS} and S about 8×10^7 times (as reported by the code when we do not use the optimized algorithm and 7.3×10^4 when we use the optimized algorithm and many \mathbf{k} -points are calculated concurrently). This is reasonable since we have 1×10^5 \mathbf{k} points, about 16 self-consistent iterations and $N_{pe} = 3$ modes. This gives an average of 16 conjugate gradient steps per iteration. To count the number of operations is more difficult since the number of bands is not always constant. If take as an average value $N_b = 11$ bands, the number of plane waves $N_{pw} = 2093$ and a number of projector functions $N_{kb} = 18$ we see that Eq. 38 is the multiplication of a matrix 18×2023 and a matrix 2023×11 . We start by considering the CPU times when FFT time is subtracted. These times depend on the number of cores, but less on how these cores are distributed between \mathbf{G} vectors and \mathbf{k} -point pools. Still using only \mathbf{k} -point pools gives the shortest times but the differences are small. Comparing with the standard GPU version, we see that the application of the nonlocal potential and of the S matrix require too many

small size matrix-matrix multiplications and this part of the calculation is quite slow on the GPU. For this calculation the required time is $6 T_{cpu}$. The optimized GPU algorithm is much faster and needs about $0.42 T_{cpu}$. Adding also the speedup obtained with the FFT, the optimized GPU algorithm takes about $0.44 T_{cpu}$. Comparing the two GPU algorithms, the optimized one is 4 times faster in applying H_{KS} and 14 times faster in applying the nonlocal pseudopotential and the S matrix.

6.5. Total time

Table 4: Total time spent in the standard CPU calculations. The number of CPUs, GPUs, tasks, and pools are also indicated. The number of core-hours is obtained multiplying the total time by the number of cores.

| CPU | | | | | | | |
|------------|-------|-------|------|------|------|------|------|
| #CPU | 32 | 32 | 32 | 64 | 64 | 128 | 256 |
| #GPU | 0 | 0 | 0 | 0 | 0 | 0 | 0 |
| #task(np) | 32 | 32 | 32 | 64 | 64 | 128 | 256 |
| #pool(nk) | 8 | 16 | 32 | 32 | 64 | 128 | 256 |
| time (s) | 11400 | 10560 | 8040 | 5640 | 4500 | 2280 | 1182 |
| time (m) | 190 | 176 | 134 | 94 | 75 | 38 | 20 |
| core-hours | 101 | 94 | 71 | 100 | 80 | 81 | 85 |

Table 5: Total time spent in the standard GPU calculations. This includes also the time passed on the part of the code that are not GPU accelerated or are not GPU optimized. The number of CPUs, GPUs, tasks, and pools are equal.

| GPU | | | | | | |
|------------|--------|-------|-------|-------|------|------|
| #CPU | 1 | 2 | 4 | 8 | 16 | 32 |
| time (s) | 107640 | 54780 | 27720 | 14100 | 7500 | 3720 |
| time (m) | 1794 | 913 | 462 | 235 | 125 | 62 |
| core-hours | 239 | 243 | 246 | 250 | 267 | 265 |

In this section we present some benchmarks of the entire run, considering both the self consistent and the phonon frequencies calculations. We report in Tables 4, 5, 6 the total time. This time is approximately twice the time required by the application of H_{KS} and S in the CPU and in the optimized GPU cases and three times in the standard GPU case. Considering now the total T_{cpu} , we see that the faster time is obtained when the number of pools is equal

Table 6: Total time spent in the optimized GPU calculations. This includes also the time passed on the part of the code that are not GPU accelerated or are not GPU optimized. The number of CPUs, GPUs, tasks, and pools are equal.

| | optimized GPU | | | | | |
|------------|---------------|------|------|------|------|-----|
| #CPU | 1 | 2 | 4 | 8 | 16 | 32 |
| time (s) | 16080 | 7860 | 4680 | 2153 | 1140 | 585 |
| time (m) | 268 | 131 | 78 | 36 | 19 | 10 |
| core-hours | 36 | 35 | 42 | 38 | 41 | 43 |

to the number of cores. The scaling with the number of nodes is good: from 32 to 64 cores the code is 1.8 times faster. The standard GPU approach takes $3.4 T_{cpu}$ (one node) or $3.1 T_{cpu}$ (two nodes), while the optimized GPU approach takes $0.58 T_{cpu}$ (one node) and $0.48 T_{cpu}$ (two nodes). The difference between one and two nodes is due to the different number of CPUs cores available in the two cases. The parts that are not accelerated are calculated faster when more cores are available. Comparing now the two GPU algorithms we see that the optimized one is about 6 times faster.

In the table we have indicated also the cost of each run in core-hours. This cost is obtained by multiplying the total time by the number of core used (in the GPU case, each GPU costs 8 cores). We have also added the time needed with 4 and 8 nodes (128 and 256 cores). We find that increasing the number of nodes the total cost tend to increase (even if there are some fluctuations) since it is difficult to achieve an exact linear scaling with the number of pools. In the optimized GPU case the optimum is obtained with 2 nodes. It is therefore convenient to carry out this calculations with a small number of nodes per \mathbf{q} point and calculate in parallel on different nodes different \mathbf{q} points and geometries. However, even with an ideal scaling with the pools and a computer that can provide as many GPUs as desired, it is still convenient to use pools that contain a number of \mathbf{k} point sufficient to occupy the GPU memory and use it (gaining about a factor 2X), than split the calculations so that each pool has a single \mathbf{k} point.

7. Conclusions and perspectives

We discussed a scheme to accelerate on the GPUs electronic structure codes based on plane waves and pseudopotentials. We have shown in the example of bcc tungsten that our scheme can be faster than the currently

implemented GPU version when the system has small unit cells but requires a thick mesh of \mathbf{k} points. The main idea is to apply the Hamiltonian to the wave-functions in parallel on many \mathbf{k} points, one per GPU thread, so as to increase both the size of the data on which the GPU works at any given time and to give to the GPU a sufficient numerical workload to exploit all its SMs. Our method has been implemented in `CUDA Fortran` by partially rewriting the code and by using `GLOBAL` and `DEVICE` routines to parallelize the work of different GPU threads. We have discussed in detail the optimization of the Davidson algorithm, the application of the Kohn and Sham Hamiltonian and of the overlap matrix S to the wave-functions, and the preconditioned conjugate gradient algorithm which is used to solve the linear system of DFPT. In our example the application of H_{KS} and S to the wave-functions accounts for about one half of the total time with CPUs and about 1/3 with the GPUs. For these operations our optimized GPU method is about 6 times faster than the standard GPU approach, and about twice as fast than the CPUs only calculation. The main limitation of the present implementation is that it does not support the reciprocal lattice vectors distribution among CPUs. It is instead possible to divide the \mathbf{k} points in pools so that different GPUs acts on different pools. Finally, we underline the fact that when the system (and the FFT mesh) becomes large enough the `cuFFT` library routines become more efficient than our `DEVICE` routines and at that point the standard approach might become more convenient.

Our approach required a precise control of the GPU threads and math libraries (with `DEVICE` functions) that can be called from inside the GPU threads. Presently not many libraries offer this functionality and we hope that, in future, optimized `DEVICE` versions of math libraries will appear together with `FORTTRAN` compatible interfaces. The substitution of our transformed routines with better optimized ones could further improve the speed of our code. As a last consideration we might ask if there are other ways to speed up the plane-waves pseudopotential codes for metallic cases as those that we need for our research. There are several option that one might explore from introducing a batched form of the FFT and of the linear algebra routines, to using new FFT GPU libraries such as `heFFTe`. [58]. If these options would solve the problem pointed out in this paper within the standard GPU scheme remains still to be investigated.

The implemented software is distributed within the GPL licence within the `thermo_pw` package. [53]

8. Appendix: GPU and CUDA Fortran

The CUDA architecture is built around a scalable array of multithreaded Streaming Multiprocessors (SMs). Each SM has a set of execution units and a set of registers and can operate on variables contained in the GPU memory. CUDA Fortran allows the allocation of data on the GPU (called DEVICE in this context), the transfer of data from and to the GPU and the writing of routines that can run on the GPU in many different threads, each one working on different data (called GLOBAL) or that can be called from the GPU threads (called DEVICE). This is possible also with OpenACC and openMP compiler directives but we have opted for CUDA Fortran since in this moment there is a large basis of installed supercomputers equipped with NVIDIA GPUs that can run code written in CUDA Fortran and also the one available to us is in this category. The use of OpenACC and openMP that could be required to make our code transferable to GPUs of other vendors might be considered in the future if necessary.

In CUDA Fortran, to run on the GPU, one declares the routines with ATTRIBUTES(GLOBAL) or ATTRIBUTES(DEVICE). Both run on the GPU, but the first can be called from the CPU host with the triple chevron syntax (<<<, >>>) to specify the number of threads blocks and threads per block that are employed. In general thread blocks can be arranged in a three dimensional grid with variable size in each dimension. The second can be called from the GLOBAL routines on the data already selected for the current thread. CUDA makes four pieces of information available to each thread: the thread index (`threadIdx`), the block index (`blockIdx`), the size and shape of a block (`blockDim`), and the size and shape of a grid (`gridDim`). This information can be used to choose the variables the current thread will work on.

To give an order of magnitude, the Volta (Ampère) GPU architecture has 84 (108) SMs each capable of running up to 32 threads that is $32 \times 84 = 2688$ (3456) threads can run simultaneously on the GPU, however each thread block must run the same instructions on different data, while different thread blocks can execute different instructions. The code is independent from the GPU architecture on which it will run and can require even bigger grids and block sizes whose threads are run in sequence on the available SMs.

9. Acknowledgments

This work has been supported by the Italian MUR (Ministry of University and Research) through the National Centre for HPC, Big Data, and Quantum Computing (grant No. CN00000013). Computational facilities have been provided by SISSA through its Linux Cluster, ITCS, and the SISSA-CINECA 2021-2024 Agreement. Partial support has been received by MAX “MATERIALS design at the eXascale” Centre of Excellence for Supercomputing applications (Grant agreement No. 101093374, co-funded by the European High Performance Computing joint Undertaking (JU) of the European Union and participating countries). X. Gong acknowledges the support received in the framework of the Joint Research Agreement for Magnetic Confinement Fusion between Eni and CNR.

References

- [1] P. Hohenberg, W. Kohn, Inhomogeneous electron gas, *Physical Review* 136 (3) (1964) B864–B871. doi:10.1103/PhysRev.136.B864.
URL <https://link.aps.org/doi/10.1103/PhysRev.136.B864>
- [2] W. Kohn, L. J. Sham, Self-consistent equations including exchange and correlation effects, *Physical Review* 140 (4) (1965) A1133–A1138. doi:10.1103/PhysRev.140.A1133.
URL <https://link.aps.org/doi/10.1103/PhysRev.140.A1133>
- [3] P. Giannozzi, S. Baroni, N. Bonini, M. Calandra, R. Car, C. Cavazzoni, D. Ceresoli, G. L. Chiarotti, M. Cococcioni, I. Dabo, A. Dal Corso, S. de Gironcoli, S. Fabris, G. Fratesi, R. Gebauer, U. Gerstmann, C. Gougoussis, A. Kokalj, M. Lazzeri, L. Martin-Samos, N. Marzari, F. Mauri, R. Mazzarello, S. Paolini, A. Pasquarello, L. Paulatto, C. Sbraccia, S. Scandolo, G. Sclauzero, A. P. Seitsonen, A. Smogunov, P. Umari, R. M. Wentzcovitch, QUANTUM ESPRESSO: a modular and open-source software project for quantum simulations of materials, *Journal of Physics: Condensed Matter* 21 (39) (2009) 395502.
- [4] P. Giannozzi, O. Andreussi, T. Brumme, O. Bunau, M. Buongiorno Nardelli, M. Calandra, R. Car, C. Cavazzoni, D. Ceresoli, M. Cococcioni, N. Colonna, I. Carnimeo, A. Dal Corso, S. de Gironcoli, P. Delugas, R. A. DiStasio, A. Ferretti, A. Floris, G. Fratesi, G. Fugallo,

- R. Gebauer, U. Gerstmann, F. Giustino, T. Gorni, J. Jia, M. Kawamura, H.-Y. Ko, A. Kokalj, E. Küçükbenli, M. Lazzeri, M. Marsili, N. Marzari, F. Mauri, N. L. Nguyen, H.-V. Nguyen, A. Otero-de-la Roza, L. Paulatto, S. Poncé, D. Rocca, R. Sabatini, B. Santra, M. Schlipf, A. P. Seitsonen, A. Smogunov, I. Timrov, T. Thonhauser, P. Umari, N. Vast, X. Wu, S. Baroni, Advanced capabilities for materials modelling with Quantum ESPRESSO, *Journal of Physics: Condensed Matter* 29 (46) (2017). doi:10.1088/1361-648X/aa8f79.
URL <https://www.osti.gov/pages/biblio/1523470>
- [5] X. Gonze, B. Amadon, G. Antonius, F. Arnardi, L. Baguet, J.-M. Beuken, J. Bieder, F. Bottin, J. Bouchet, E. Bousquet, N. Brouwer, F. Bruneval, G. Brunin, T. Cavignac, J.-B. Charraud, W. Chen, M. Côté, S. Cottenier, J. Denier, G. Geneste, P. Ghosez, M. Giantomassi, Y. Gillet, O. Gingras, D. R. Hamann, G. Hautier, X. He, N. Helbig, N. Holzwarth, Y. Jia, F. Jollet, W. Lafargue-Dit-Hauret, K. Lejaeghere, M. A. L. Marques, A. Martin, C. Martins, H. P. C. Miranda, F. Naccarato, K. Persson, G. Petretto, V. Planes, Y. Pouillon, S. Prokhorenko, F. Ricci, G.-M. Rignanese, A. H. Romero, M. M. Schmitt, M. Torrent, M. J. van Setten, B. V. Troeye, M. J. Verstraete, G. Zérah, J. W. Zwanziger, The abinit project: Impact, environment and recent developments, *Comput. Phys. Commun.* 248 (2020) 107042. URL <https://doi.org/10.1016/j.cpc.2019.107042>
- [6] G. Kresse, D. Joubert, From ultrasoft pseudopotentials to the projector augmented-wave method, *Phys. Rev. B* 59 (1999) 1758–1775. doi:10.1103/PhysRevB.59.1758.
URL <https://link.aps.org/doi/10.1103/PhysRevB.59.1758>
- [7] S. J. Clark, M. D. Segall, C. J. Pickard, P. J. Hasnip, M. I. J. Probert, K. Refson, M. C. Payne, First principles methods using CASTEP, *Zeitschrift für Kristallographie - Crystalline Materials* 220 (5-6) (2005) 567–570. doi:doi:10.1524/zkri.220.5.567.65075.
URL <https://doi.org/10.1524/zkri.220.5.567.65075>
- [8] R. C. Walker, A. W. Götz (Eds.), *Electronic Structure Calculations on Graphics Processing Units: From Quantum Chemistry to Condensed Matter Physics*, John Wiley & Sons, Ltd, 2016. doi:10.1002/9781118670712.

- [9] P. Giannozzi, O. Basergio, P. Bonfà, D. Brunato, R. Car, I. Carnimeo, C. Cavazzoni, S. de Gironcoli, P. Delugas, F. Ferrari Ruffino, A. Ferretti, N. Marzari, I. Timrov, A. Urru, S. Baroni, Quantum ESPRESSO toward the exascale, *The Journal of Chemical Physics* 152 (15) (2020) 154105. doi:10.1063/5.0005082.
URL <https://doi.org/10.1063/5.0005082>
- [10] M. Smith, A. Tamerus, P. Hasnip, Portable acceleration of materials modeling software: CASTEP, GPUs, and OpenACC, *Computing in Science & Engineering* 24 (1) (2022) 46–55. doi:10.1109/MCSE.2022.3141714.
URL <https://ieeexplore.ieee.org/document/9676479>
- [11] O. Schütt, P. Messmer, J. Hutter, J. VandeVondele, GPU-Accelerated Sparse Matrix–Matrix Multiplication for Linear Scaling Density Functional Theory, John Wiley & Sons, Ltd, 2016, Ch. 8, pp. 173–190. doi:<https://doi.org/10.1002/9781118670712.ch8>.
URL <https://onlinelibrary.wiley.com/doi/abs/10.1002/9781118670712.ch8>
- [12] GPU support in Abinit is mentioned here: (2024).
URL https://docs.abinit.org/INSTALL_gpu/
- [13] OpenACC GPU port of VASP.6.2.0 is mentioned here:.
URL https://www.vasp.at/wiki/index.php/OpenACC_GPU_port_of_VASP
- [14] NVIDIA, P. Vingelmann, F. H. Fitzek, CUDA, release: 10.2.89 (2020).
URL <https://developer.nvidia.com/cuda-toolkit>
- [15] OpenACC-Standard.org, The openacc application programming interface ver 3.3 (2022).
URL <https://https://www.openacc.org>
- [16] D. Datta, M. S. Gordon, Accelerating coupled-cluster calculations with GPUs: An implementation of the density-fitted CCSD(t) approach for heterogeneous computing architectures using OpenMP directives, *Journal of Chemical Theory and Computation* 19 (21) 7640–7657. doi:10.1021/acs.jctc.3c00876.

- [17] F. F. Ruffino, L. Bellentani, G. Rossi, F. Affinito, S. Baroni, O. Baseggio, P. Delugas, P. Giannozzi, J. Kurzak, Y. Luo, O. O'Reilly, S. Orlandini, I. Carnimeo, Quantum ESPRESSO towards performance portability: GPU offload with OpenMP, *Procedia Computer Science* 240 (2024) 52–60. doi:10.1016/j.procs.2024.07.008.
- [18] Nvidia Corp., cuBLAS, the cuda basic linear algebra subroutine library (2024).
URL <https://docs.nvidia.com/cuda/cublas/index.html>
- [19] Nvidia Corp., cuSOLVER, a gpu accelerated library for decompositions and linear system solutions for both dense and sparse matrices (2024).
URL <https://docs.nvidia.com/cuda/cusolver/index.html>
- [20] Nvidia Corp., cuFFT API Reference v12.4 (2024).
URL <https://docs.nvidia.com/cuda/cufft/index.html>
- [21] MAGMA.
URL <https://icl.utk.edu/magma/>
- [22] M. Hutchinson, P. Fleurat-Lessard, A. Anciaux-Sedrakian, D. Stosic, J. Bédorf, S. Tariq, *Plane-Wave Density Functional Theory*, John Wiley & Sons, Ltd, 2016, Ch. 7, pp. 135–172. arXiv:<https://onlinelibrary.wiley.com/doi/pdf/10.1002/9781118670712.ch7>, doi:<https://doi.org/10.1002/9781118670712.ch7>.
URL <https://onlinelibrary.wiley.com/doi/abs/10.1002/9781118670712.ch7>
- [23] W. P. Huhn, B. Lange, V. W.-z. Yu, M. Yoon, V. Blum, GPU acceleration of all-electron electronic structure theory using localized numeric atom-centered basis functions, *Computer Physics Communications* 254 (2020) 107314. doi:10.1016/j.cpc.2020.107314.
- [24] J.-L. Fattebert, C. F. A. Negre, J. Finkelstein, J. Mohd-Yusof, D. Osei-Kuffuor, M. E. Wall, Y. Zhang, N. Bock, S. M. Mniszewski, Hybrid programming-model strategies for GPU offloading of electronic structure calculation kernels, *The Journal of Chemical Physics* 160 (12) (2024) 122501. doi:10.1063/5.0198797.
- [25] S. Das, P. Motamarri, V. Subramanian, D. M. Rogers, V. Gavini, DFT-FE 1.0: A massively parallel hybrid CPU-GPU density functional theory

- code using finite-element discretization, *Computer Physics Communications* 280 (2022) 108473. doi:10.1016/j.cpc.2022.108473.
- [26] F. Spiga, I. Girotto, phiGEMM: A CPU-GPU Library for Porting Quantum ESPRESSO on Hybrid Systems, in: 2012 20th Euromicro International Conference on Parallel, Distributed and Network-based Processing, 2012, pp. 368–375. doi:10.1109/PDP.2012.72.
- [27] J. Romero, E. Phillips, G. Ruetsch, M. Fatica, F. Spiga, P. Giannozzi, A Performance Study of Quantum ESPRESSO’s PWscf Code on Multi-core and GPU Systems, in: S. Jarvis, S. Wright, S. Hammond (Eds.), *High Performance Computing Systems. Performance Modeling, Benchmarking, and Simulation*, Springer International Publishing, Cham, 2018, pp. 67–87. doi:10.1007/978-3-319-72971-8_4.
- [28] M. Methfessel, A. T. Paxton, High-precision sampling for brillouin-zone integration in metals, *Physical Review B* 40 (1989) 3616–3621. doi:10.1103/PhysRevB.40.3616.
URL <https://link.aps.org/doi/10.1103/PhysRevB.40.3616>
- [29] X. Gong, A. Dal Corso, Pressure and temperature dependent ab-initio quasi-harmonic thermoelastic properties of tungsten, *Journal of Physics: Condensed Matter* 36 (28) (2024) 285702. doi:10.1088/1361-648X/ad3ac3.
URL <https://dx.doi.org/10.1088/1361-648X/ad3ac3>
- [30] X. Gong, A. Dal Corso, Ab initio quasi-harmonic thermoelasticity of molybdenum at high temperature and pressure, *The Journal of Chemical Physics* 160 (24) (2024) 244703. doi:10.1063/5.0212162.
- [31] C. Malica, A. Dal Corso, Quasi-harmonic temperature dependent elastic constants: applications to silicon, aluminum, and silver, *Journal of Physics: Condensed Matter* 32 (31) (2020) 315902.
- [32] C. Malica, A. Dal Corso, Quasi-harmonic thermoelasticity of palladium, platinum, copper, and gold from first principles, *Journal of Physics: Condensed Matter* 33 (47) (2021) 475901.
- [33] B. Thakur, X. Gong, A. Dal Corso, Ab initio thermodynamic properties of iridium: A high-pressure and high-temperature

- study, *Computational Materials Science* 234 (2024) 112797. doi:10.1016/j.commatsci.2024.112797.
URL <https://www.sciencedirect.com/science/article/pii/S0927025624000181>
- [34] B. Thakur, X. Gong, A. Dal Corso, Thermodynamic properties of rhodium—a first principle study, *AIP Advances* 14 (4) (2024) 045229. doi:10.1063/5.0203098.
URL <https://doi.org/10.1063/5.0203098>
- [35] A. Dal Corso, Elastic constants of beryllium: a first-principles investigation, *Journal of Physics: Condensed Matter* 28 (7) (2016) 075401.
- [36] X. Gong, A. Dal Corso, High-temperature and high-pressure thermoelasticity of hcp metals from ab initio quasiharmonic free energy calculations: The beryllium case, *Physical Review B* 110 (9) (2024) 094109. doi:10.1103/PhysRevB.110.094109.
- [37] Nvidia Corp., The cufft device extensions (cufftdx) library (2022).
URL <https://docs.nvidia.com/cuda/cufftdx/index.html>
- [38] L. Kleinman, D. M. Bylander, Efficacious form for model pseudopotentials, *Physical Review Letters* 48 (20) (1982) 1425–1428. doi:10.1103/PhysRevLett.48.1425.
URL <https://link.aps.org/doi/10.1103/PhysRevLett.48.1425>
- [39] D. Vanderbilt, Soft self-consistent pseudopotentials in a generalized eigenvalue formalism, *Physical Review B* 41 (1990) 7892–7895. doi:10.1103/PhysRevB.41.7892.
URL <https://link.aps.org/doi/10.1103/PhysRevB.41.7892>
- [40] P. E. Blöchl, Projector augmented-wave method, *Physical Review B* 50 (24) (1994) 17953–17979. doi:10.1103/PhysRevB.50.17953.
URL <https://link.aps.org/doi/10.1103/PhysRevB.50.17953>
- [41] G. Kresse, D. Joubert, From ultrasoft pseudopotentials to the projector augmented-wave method, *Physical Review B* 59 (3) (1999) 1758–1775. doi:10.1103/PhysRevB.59.1758.
URL <https://link.aps.org/doi/10.1103/PhysRevB.59.1758>

- [42] E. R. Davidson, The iterative calculation of a few of the lowest eigenvalues and corresponding eigenvectors of large real-symmetric matrices, *Journal of Computational Physics* 17 (1) (1975) 87–94. doi:10.1016/0021-9991(75)90065-0.
- [43] E. Anderson, Z. Bai, C. Bischof, S. Blackford, J. Demmel, J. Dongarra, J. Du Croz, A. Greenbaum, S. Hammarling, A. McKenney, D. Sorensen, *LAPACK Users' Guide*, 3rd Edition, Society for Industrial and Applied Mathematics, Philadelphia, PA, 1999.
- [44] W. E. Pickett, Pseudopotential methods in condensed matter applications, *Computer Physics Reports* 9 (3) (1989) 115–197. doi:10.1016/0167-7977(89)90002-6.
URL <https://www.sciencedirect.com/science/article/pii/0167797789900026>
- [45] S. Baroni, S. de Gironcoli, A. Dal Corso, P. Giannozzi, Phonons and related crystal properties from density-functional perturbation theory, *Reviews of Modern Physics* 73 (2) (2001) 515–562, publisher: American Physical Society. doi:10.1103/RevModPhys.73.515.
URL <https://link.aps.org/doi/10.1103/RevModPhys.73.515>
- [46] A. Dal Corso, Density-functional perturbation theory with ultrasoft pseudopotentials, *Physical Review B* 64 (2001) 235118. doi:10.1103/PhysRevB.64.235118.
URL <https://link.aps.org/doi/10.1103/PhysRevB.64.235118>
- [47] W. H. Press, S. A. Teukolsky, W. T. Vetterling, B. P. Flannery, *Numerical recipes in FORTRAN 90: the art of parallel scientific computing*, 2nd Edition, Cambridge University Press, 1996.
- [48] M. Hestenes, E. Stiefel, Methods of conjugate gradients for solving linear systems, *Journal of Research of the National Bureau of Standards* 49 (6) 409. doi:10.6028/jres.049.044.
URL https://nvlpubs.nist.gov/nistpubs/jres/049/jresv49n6p409_A1b.pdf
- [49] G. Fugallo, M. Lazzeri, L. Paulatto, F. Mauri, Ab initio variational approach for evaluating lattice thermal conductivity, *Physical Review*

- B 88 (4) (2013) 045430. doi:10.1103/PhysRevB.88.045430.
 URL <https://link.aps.org/doi/10.1103/PhysRevB.88.045430>
- [50] M. P. Teter, M. C. Payne, D. C. Allan, Solution of schrödinger's equation for large systems, *Physical Review B* 40 (18) 12255–12263. doi:10.1103/PhysRevB.40.12255.
 URL <https://link.aps.org/doi/10.1103/PhysRevB.40.12255>
- [51] M. Frigo, S. G. Johnson, The design and implementation of FFTW3, *Proceedings of the IEEE* 93 (2) (2005) 216–231, special issue on “Program Generation, Optimization, and Platform Adaptation”.
- [52] D. Valent, P. Swarztrauber, FFTPACK 5.1 (2022).
 URL https://people.sc.fsu.edu/~jburkardt/f77_src/fftpack5.1/fftpack5.1.html
- [53] A. Dal Corso, THERMO_pw can be found at the webpage https://dalcorso.github.io/thermo_pw/ (Mar. 2014).
- [54] J. P. Perdew, A. Ruzsinszky, G. I. Csonka, O. A. Vydrov, G. E. Scuseria, L. A. Constantin, X. Zhou, K. Burke, Restoring the density-gradient expansion for exchange in solids and surfaces, *Physical Review Letters* 100 (2008) 136406. doi:10.1103/PhysRevLett.100.136406.
 URL <https://link.aps.org/doi/10.1103/PhysRevLett.100.136406>
- [55] A. Dal Corso, pslibrary, can be found at the webpage <https://github.com/dalcorso/pslibrary> (Mar. 2010).
- [56] Message Passing Interface Forum, MPI: A Message-Passing Interface Standard Version 4.0 (jun 2021).
 URL <https://www.mpi-forum.org/docs/mpi-4.0/mpi40-report.pdf>
- [57] Nvidia Corp., NVIDIA HPC SDK Version 23.7 Documentation (2023).
 URL <https://docs.nvidia.com/hpc-sdk/archive/23.7/>
- [58] U. o. T. Innovative Computing Laboratory (ICL), the highly efficient fft for exascale (heffte) library (2024).
 URL <https://icl.utk.edu/fft/>